

PACS numbers: 42.62.Cf
DOI: 10.1070/QE2006v036n07ABEH013181

Mechanism of laser drilling superhigh-aspect-ratio holes in polymers

V.N. Tokarev

***Abstract*. A brief review of recent theoretical and experimental studies of multipulse laser drilling keyholes in polymers is presented. The stationary keyhole profile is obtained after irradiation by a quite great number of laser pulses due to self-organisation processes and is a new more stable state of the surface irradiated by intense light. This concept together with ample experimental data obtained for various polymers form the basis of the analytical model of multipulse drilling holes with a superhigh depth – diameter ratio (300 – 600) (the so-called aspect ratio) by using UV excimer KrF laser radiation. The model reveals the main factors controlling the parameters of drilling holes by nanosecond UV pulses and, in particular, determines the conditions for drilling holes with virtually parallel side walls and very high aspect ratios.**

Keywords: *laser drilling, simulation, hole profile, polymers, beam divergence, optimal drilling conditions, superhigh aspect ratio.*

1. Review of the literature and formulation of the problem

The laser drilling (LD) of microholes of diameters from a few micrometers to a few hundreds of micrometers is widely used, in particular, in microelectronics for drilling polymer boards for microcircuits (see, for example, [1, 2]), texturing magnetic hard disks, video heads [3], and diamond films; in aerospace and automobile industry for drilling precise fields of small holes in hard refractory metal and alloys (for example, cooling holes in gas turbine vanes), drilling hard refractory ceramics Al_2O_3, ZrO_2, Si_3N_4, SiC, and AlN, for example, in the manufacturing of nozzles for injecting fuels in prospective ceramic engines; in clock and medical industries, as well as in jewellery practice for drilling and microprocessing diamond, ruby, and other jem stones [4 – 14].

Laser drilling has been studied and applied by using a variety of IR, visible, and UV lasers operating both in cw and pulsed regimes with pulse durations in the milli-, nano-, pico-, and subpicosecond ranges. Nanosecond UV lasers considered in this paper attract particular attention because it has been found experimentally that upon drilling important modern technological materials such as polymers and very hard refractory ceramics these lasers provide the unprecedented reproducibility of the results from hole to hole on the surface being irradiated along with the high spatial resolution, accuracy, and quality, which cannot be achieved with IR and visible lasers (see, for example, [1 – 8, 10 – 13]). A relatively small depth of material removal per nanosecond laser pulse (~ 1 μm and smaller) means that a few thousands of nanosecond pulses are required to drill holes of depth of several millimetres. This problem can be solved by using high pulse repetition rates. For example, modern copper vapour lasers provide pulse repetition rates from 5 to 10 kHz, excimer lasers have the pulse repetition rate up to 1 kHz, and diode-pumped Nd : YAG lasers emit 355-nm and 266-nm pulses at pulse repetition rates of a few kilohertz.

There are two problems impairing considerably the quality of nanosecond UV LD:

(i) The holes drilled by a laser are not cylindrical, as a rule, and narrow down with depth in a material;

(ii) the aspect ratio (the ratio of the hole depth to its diameter) for metals and ceramics does not exceed 10 – 16 in many cases.

These disadvantages make the results of drilling unacceptable for some applications. The 'blind' empirical search for optimal drilling results by the trial-and-error method in each particular situation is often expensive, time-consuming, and inefficient because of a great number of parameters affecting the LD result. These parameters are the thermal and optical constants of materials, the laser pulse intensity, duration, wavelength, etc., the angular divergence of radiation focused on a surface, the size of the irradiated spot, the reduction coefficient of a mask and its diameter in the projection scheme, the beam compression or expansion coefficient, the focal distance of a lens, the position of the beam focus with respect to the irradiated surface, etc. In addition, the physicochemical structure of a target, a particular mechanism of material removal, the initial temperature of a sample, and physical and chemical parameters of the surrounding gas (its pressure, chemical activity, etc.) are also important. For example, experimental conditions were found empirically for drilling holes with the aspect ratio above 100 in polymers by UV radiation [13 – 15] and in steel and ceramics by 1.06-μm laser pulses [16, 17]. However, the mechanism of producing such high aspect ratios in both cases remained unknown.

V.N. Tokarev Natural Sciences Center, A.M. Prokhorov General Physics Institute, Russian Academy of Sciences, ul. Vavilova 38, 119991 Moscow, Russia; e-mail: tokarev@kapella.gpi.ru

Received 3 April 2006; revision received 25 May 2006
Kvantovaya Elektronika **36** (7) 624 – 637 (2006)
Translated by M.N. Sapozhnikov

The numerical computer simulation gives the result only for a particular set of parameters (see, for example, [18 – 21]) but, unfortunately, it does not allow one to estimate the situation in general in order to understand how far we are from the optimal result.

Instead of the 'blind' empirical search, it is desirable to have the general clear algorithm for optimising nanosecond multipulse UV LD, which can be used for a variety of materials and radiation and focusing parameters. Such an algorithm could be based on the analytical model describing drilling holes with high and superhigh aspect ratios. An advantage of the analytical method over numerical computer calculations is that this method gives the parameters of the final 'stationary' profile of a laser hole in the explicit form, which allows one to observe easily their variations depending on materials and focusing and radiation parameters, and to elucidate the main factors controlling the drilling process, in particular, to understand the reasons preventing drilling superhigh-aspect-ratio holes with virtually parallel side walls and to find the way to eliminate them. All this would allow one to optimise quite easily the laser drilling process and to derive, for example, explicit analytical conditions for matching the laser intensity and its distribution and the focusing and material parameters, which would provide drilling keyholes with superhigh aspect ratios (for example, a few hundreds) and virtually parallel side walls.

Although LD has been studied in many experimental and theoretical papers over more than three decades (see, for example, [1 – 30]), such an analytical model of nanosecond UV LD has not been constructed until our papers [31 – 33]. The reason was the absence of a clear understanding of the interaction processes between intense laser radiation and a laser keyhole.

In this paper, we describe an analytical mathematical model which well agrees with the experimental results obtained for polymers. For drilling superhigh-aspect-ratio holes considered here, it is very important to take into account the two key factors:

(i) Mechanism of energy propagation and absorption in laser superhigh-aspect-ratio keyholes. This mechanism depends on the roughness of the inner surface of the hole. If the surface roughness is small, multiple specular reflections of laser beams from the walls can dominate, whereas in the case of a considerable roughness, diffusion scattering can dominate [18]. The value of roughness, in turn, depends on numerous factors (for example, on multiply repeated cycles of material evaporation and deposition in the form of vapour, droplets, and clusters in a deep hole growing in length and various instabilities of the melt surface layer relief on the walls of the hole in the presence of a powerful laser-plasma flux [22, 23], etc.), which makes impossible to calculate the roughness theoretically within the framework of the model. Therefore, it is also impossible to predict purely theoretically the mechanism of radiation propagation and absorption inside the hole. This mechanism can be elucidated only based on experimental results. However, such an approach has not been used in previous papers on simulations of nanosecond UV LD [18 – 21]. Moreover, the mechanism of energy propagation and absorption inside a laser-drilled hole was not considered at all in some papers and it was assumed that the laser beam was completely absorbed during the first contact with the side walls of the hole [19 – 21]. This assumption is physically absurd because it follows from Fresnel formulas that the absorption of radiation incident on the side walls at the grazing angle is very weak, amounting only to a few percent or fractions of percent, but by no means 100 %. Based on the extensive experimental results obtained for various polymers [13 – 15, 31 – 33], we elucidate in this paper a specific mechanism of energy propagation and absorption in deep superhigh-aspect-ratio laser-drilled holes.

(ii) Angular divergence of a focused laser beam. This factor was considered earlier only in paper [21], where the LD of low-aspect-ratio (smaller than 4) holes was numerically simulated. The consideration of this factor for superhigh-aspect-ratio (300 – 600) holes within the framework of the analytical model performed in our paper gave a number of substantially new results. In particular, we predicted the angular distribution of the laser beam providing drilling superhigh-aspect-ratio holes with strictly cylindrical side walls. Note for comparison that, if the angular divergence is neglected and the incident radiation is treated as a parallel beam, model calculations inevitably predict only conic holes, narrowing down deep in the material [19, 20, 30].

2. Experimental studies of LD in polymers

A high-intensity beam was produced by using a projection scheme consisting of condenser lens (*1*) with the focal distance $f = 300$ mm, mask (*2*), and projecting lens (*3*) with $f = 25$ mm (Figs 1 and 2) [13 – 15, 32, 33]. The image of the circular molybdenum mask of diameter 0.5 mm reduced five-fold by lens (*3*) was projected on the surface of material (*4*). A Lambda Physik LPX 220i excimer laser emitting 350-mJ, 25-ns pulses at 248 nm with a pulse repetition rate of up to 200 Hz was used. If necessary, only the central part of the laser beam was selected with the help of an aperture.

We studied LD in the following polymers: polyimide (PI), polyethylene terephthalate (PET), polystyrene (PS), polyether ether ketone (PEEK), polymethyl methacrylate (PMMA), and bisphenol A polycarbonate (PC) [13 – 15, 32, 33]. Their chemical structural formulas are shown in Fig. 3. All these polymers are transparent in the visible spectral region, which allows us to observe easily drilled holes with an optical microscope and to measure rapidly their parameters, in particular, to perform the real-time monitoring of the microdrilling rate from pulse to

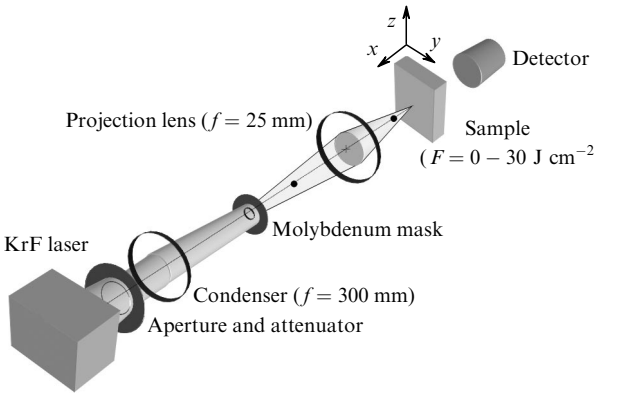

Figure 1. Projection scheme of the hole-drilling experiment. All the angles are strongly enlarged for clearness.

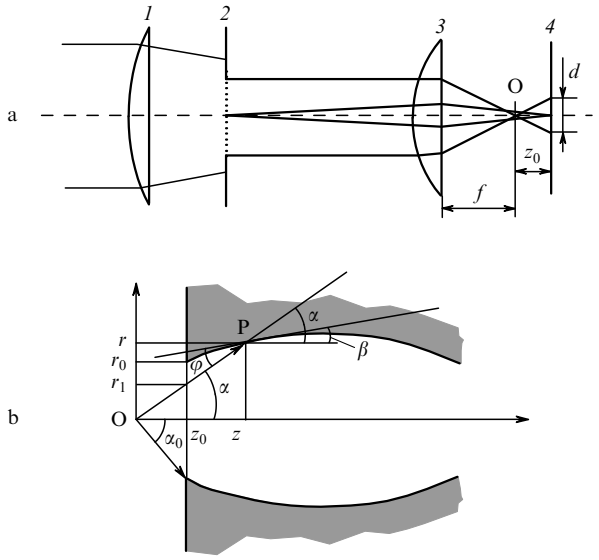

Figure 2. (a) Optical scheme for drilling holes by using a projection scheme [(*1*) condenser lens; (*2*) molybdenum mask; (*3*) projecting lens; (*4*) material surface] and (b) one of the rays OP of the incident beam inside the hole. All the angels are strongly enlarged for clearness.

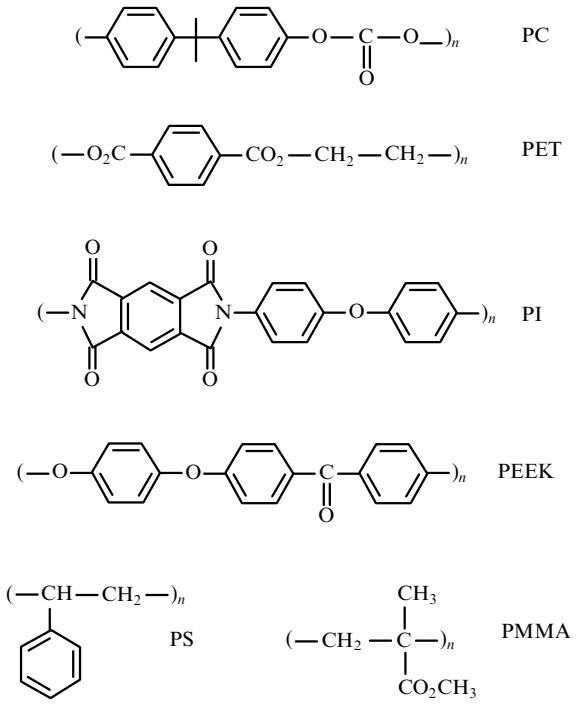

Figure 3. Structural formulas of polymers under study: bisphenol A polycarbonate (PC), polyethylene terephthalate (PET, maylar), polyimide (PI), polyether ether ketone (PEEK), polystyrene (PS), and polymethyl methacrylate (PMMA).

pulse and accumulate also other experimental data for these materials.

One can see from Table 1 that PI, PET, and PEEK have high initial room-temperature absorption coefficients at the UV laser wavelength used in experiments, whereas the absorption coefficients of PMMA, PS, and PC are low, which allows us to study the influence of this parameter on the results of drilling.

The ablation thresholds for polymers under study are low compared to those for metals and ceramics. This allows high-aspect-ratio holes (for example, 600 for PET) to be drilled even at comparatively low laser energy densities (less than 7 J cm^{-2}), when the influence of the laser plasma on the heating of the hole walls and, therefore, on the results of drilling, which is difficult to study and simulate, is minimised to a great extent. It considerably simplifies the construction of the model. Note that this is not the case for drilling holes in metals and ceramics by laser pulses with the same wavelength and duration as for polymers. For the energy densities used for drilling deep holes in these materials (typically, above 50 J cm^{-2}), the influence of the laser plasma cannot be neglected, which considerably complicates the construction of the drilling model.

Superhigh-aspect-ratio holes drilled by a laser in PMMA are shown in Fig. 4a (the hole length and diameter are 500 and 8 μm, respectively) and in PET in Fig. 4b (a series of holes with the input diameter ~ 35 μm drilled for laser energy densities from 1 to 20 J cm^{-2}) [32, 33].

Figure 5 presents the surface morphology on the input plane of holes drilled in PC and PMMA. This figure demonstrates the influence of a material on the depth and quality of drilled holes. In the case of PMMA, the front plane of the sample is covered with many frozen droplets, while the side walls of the hole are rough to a great extent. The quality of holes drilled in PC is much better: no

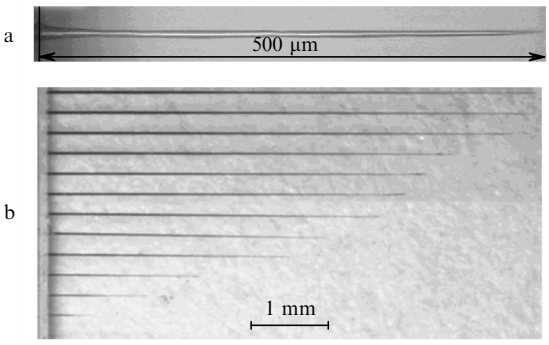

Figure 4. (a) High-aspect-ratio hole drilled in PMMA by a 248-nm laser (the hole length and input diameter are 500 and 8 μm, respectively) and (b) a series of holes drilled in PET by a 248-nm laser (the input hole diameter is 35 μm) at laser energy densities $F = 1 - 20$ J cm^{-2} to obtain the dependence of the hole depth on the energy density shown in Fig. 9.

Table 1. Parameters of absorption (for low radiation intensity), ablation, and drilling for polymers at a wavelength of 248 nm.

Parameters	PMMA	PI	PC	PET	PS	PEEK
Absorption coefficient $\gamma/\mu m^{-1}$	0.0063	22	1	16	0.61	~ 10
Radiation penetration depth $\gamma^{-1}/\mu m$	150	0.045	1.0	0.065	1.6	~ 0.1
Ablation threshold $F_{th}/mJ\ cm^{-2}$	250	54	40	30	40	50
Threshold F_{st} of material removal from walls upon drilling/mJ cm^{-2}	6.6	3	2.2	1	5	8.5
Drilling rate/μm $pulse^{-1}$	2.5	0.4	0.8	0.7	–	0.6
Maximal aspect ratio	255	360	390	565	315	385

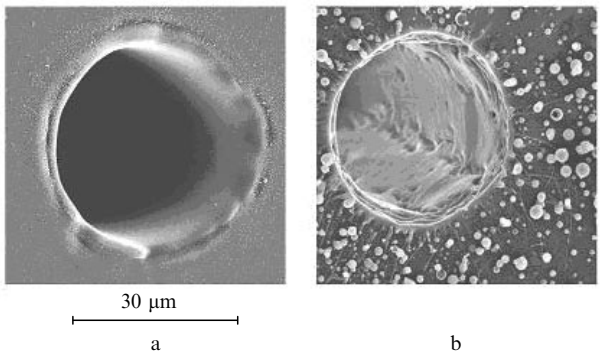

Figure 5. Surface morphology near the entrance to a hole drilled by a laser in (a) PC (the input diameter of the hole and its length are 30 μm and 5 mm, respectively) and (b) PMMA (the input diameter of the hole and its length are 30 μm and 2 mm, respectively). The surface is covered by dropletlets formed due to the ejection of the melt from the hole during drilling.

droplets are observed on the front plane and the roughness of side walls is much weaker. It is known that PC gives the so-called dry ablation, i.e., ablation without the formation of droplets. These results show that the ejection of the melt in some cases, for example, in PMMA can substantially contribute to the drilling rate.

The experimental dependence of the drilling rate on the number of laser pulses (Fig. 6) has three regions corresponding to three stages: ablation in a shallow spot where the drilling rate depends on the incident energy density, ablation in a deep hole where the dense plasma and a strong attenuation of the laser beam result in a constant drilling rate of about 1 μm pulse^{-1} and, finally, a spontaneous termination of drilling when a certain depth of the hole is achieved and the next laser pulses do not increase the depth of the so-called stationary hole [14, 32]. The presence of these stages is explained by the model proposed below.

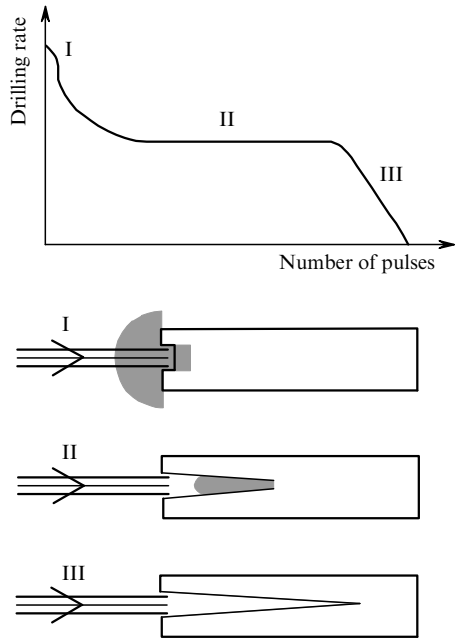

Figure 6. Dependence of the drilling rate on the number of laser pulses consisting of three regions: (I) surface ablation in a shallow hole (the drilling rate depends on the energy density); (II) ablation in a deep hole (dense plasma and strong attenuation of the laser beam, the drilling rate is constant); (III) spontaneous stop of microdrilling in a deep hole after irradiation by some number of pulses.

Figure 7 shows photographs obtained with an optical microscope which demonstrate the change in the hole profile after irradiation by 3500, 4500, 6000, and 7500 pulses [33]. After irradiation by 7500 pulses, the stationary profile and depth are achieved which do not change upon further irradiation – drilling stops spontaneously. It is interesting that the end of the hole in the stationary profile has a sharpened shape.

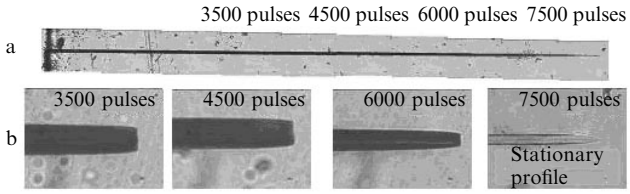

Figure 7. (a) Stationary profile of the hole obtained in PET (the input diameter of the hole and its length are 25 μm and 4.5 mm, respectively, and the aspect ratio is 180) after irradiation by 7500 laser pulses (the hole depths are indicated after irradiation by 3500, 4500, 6000, and 7500 pulses) and (b) profiles of the hole near the bottom after irradiation by 3500, 4500, 6000, and 7500 pulses (after irradiation by 7500 pulses, the stationary profile and depth are achieved, which do not change during further drilling and drilling stops spontaneously). Photographs were obtained with an optical microscope.

Note also that optical-microscope photographs in Fig. 8 show that, although the profile of the high-aspect-ratio hole narrows down near the hole end, there exists a long region where the side walls of the hole are virtually parallel [33].

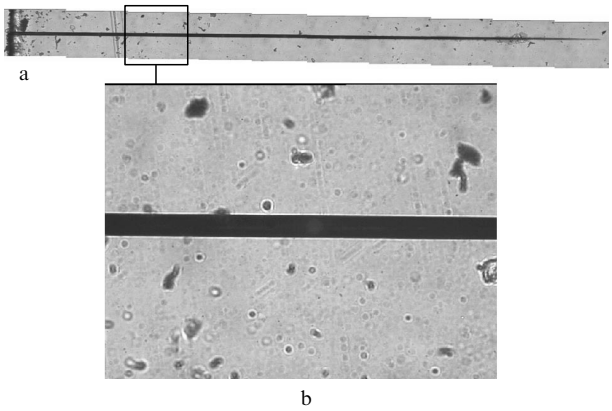

Figure 8. (a) Same stationary profile of the high-aspect-ratio hole in PET as in Fig. 7a and (b) a part of this profile with virtually parallel side walls of the hole. Photographs were obtained with an optical microscope.

Figure 9 shows the experimental dependences of the depth of final holes on the laser energy density for each of the polymers under study compared with the model curves [32]. The maximum hole depth ($\sim$ 22 mm) obtained for PET corresponds to the aspect ratio $\sim$ 600. The maximum aspect ratios achieved in other polymers are smaller and strongly depend on the polymer (Table 1).

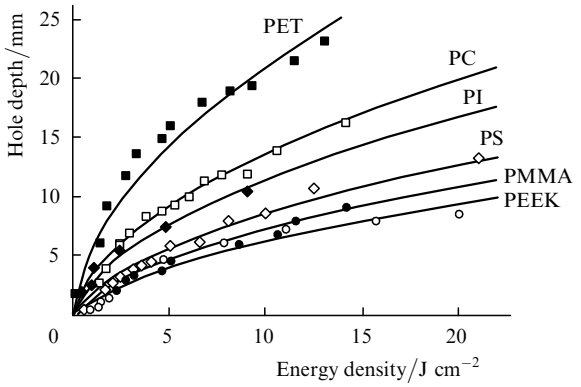

Figure 9. Experimental dependences (points) of the depth of final holes on the laser energy density compared with model dependences (solid curves) for polymers under study. The values of F_{st} used in model calculations according to (21) are 1, 2.2, 3, 5, 6.6, and 8.5 mJ cm^{-2} for PET, PC, PI, PS, PMMA, and PEEK, respectively.

The transmission of a laser beam by a through hole depending on its depth for PET, PC, and PMMA is shown in Fig. 10. The aim of this experiment was to study the properties of laser energy propagation inside the hole. For this purpose, we drilled with a laser a series of identical holes in a polymer sheet under the same conditions and then cut a triangle sample (see the inset in Fig. 10). The through holes drilled in this way had the same input diameters but different lengths and correspondingly different output diameters. The measurement of energy at the output of each of these through holes gives the dependence of transmission on the length of the hole. The transmission was measured by using the laser beam with the same parameters as for drilling. One can see that in all cases (for PET, PC, and PMMM) the transmission linearly decreases with the depth of the hole, the slope of the straight lines being dependent on the material [14] and the laser energy density used for drilling.

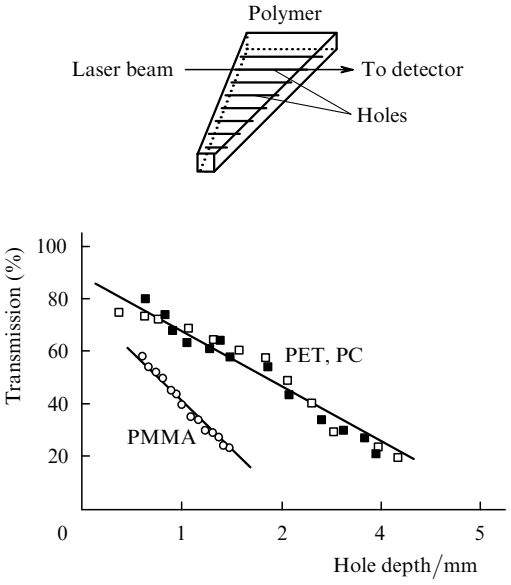

Figure 10. Transmission of the laser beam energy by a through hole (the ratio of the energy transmitted by a through hole to the incident energy) as a function of the hole depth for PET (■), PC (○), and PMMA (□).

Figure 11 shows the laser-affected region in the material around the hole drilled in PMMA. These data [14] were obtained by recording the vibrational band of the C=C bond by the confocal micro-Raman scattering [34]. This bond appeared due to the laser-induced modification of the polymer: the extracatenary and catenary dissociation of chemical bonds in the PMMA molecule. The depth of the laser-affected region is constant along the main part of of the length of the side walls of the hole. The only exception is the region near the bottom of the hole along which this depth strongly decreases. The penetration depth of radiation in other polymers is much smaller (2 μm for PET and 5 μm for PC and PS). As a result, the depths of laser-affected regions cannot be accurately measured by the method of Raman scattering.

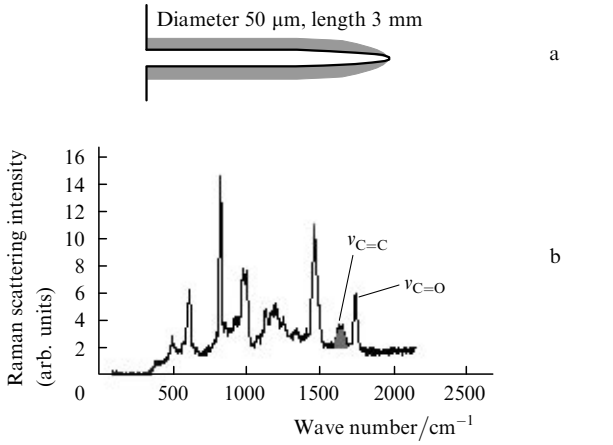

Figure 11. Laser-affected region around the hole profile (a) measured in PMMA by detecting the vibrational band of the C=C bond by the confocal micro-Raman scattering (b); $\nu_{C=O}$ is the line frequency invariable during repeated laser irradiation; $\nu_{C=C}$ is the frequency of a new line appearing after irradiation.

3. Drilling model taking into account the angular divergence of a laser beam

We will describe the profile of a hole drilled with a laser beam with the axially symmetric intensity distribution (Figs 1 and 2a) in the cylindrical coordinate system (Fig. 2b). Let us assume that $z = 0$ corresponds to the position of the laser beam focus and $z = z_0$ to the front plane of a sample which is located in the region $z \geqslant z_0$. According to the projection scheme used in experiments (Figs 1 and 2a), similarly to a Gaussian beam considered below in section 3.5 (see Fig. 16), our beam has a diffraction waist, which is characterised by a minimum non-zero radius (at $z = 0$) and a length z_R. We assume for convenience of calculations that a sample is located outside the waist (i.e., $z_0 > z_R$), similarly to the situation with a Gaussian beam. This means that different rays of our beam incident on the side walls of the hole can be treated as rays coming from a point source located at the point $z = 0$ and having the angular divergence, for example, $\alpha_0 = r_0/z_0$ for the rectangular spatial profile of the beam, where r_0 is the radius of the laser spot on the input plane of the sample.

The laser drilling of deep holes by cw radiation or long (millisecond) single pulses was investigated earlier in many

papers (see, for example, [24–28]). Here, we consider another regime of multipulse drilling by shorter nanosecond pulses. A comparatively small depth of material removal during such a pulse (~ 1 μm and smaller) means that a few thousands of pulses are required to drill holes of depth of several millimetres. Therefore, variations in the hole profile from pulse to pulse are extremely small. For example, to drill a hole in a 1-mm thick plate made of a metal, ceramics, or polymer at the ablation rate of 0.2 μm pulse^{-1} or smaller [typical ablation rate for a nanosecond pulse (see, for example, [9, 14, 15, 33])], approximately 5000 or more pulses are required. The profile of the hole is controlled in this case by self-regulation and self-organisation processes, and it is important to take into account the fact that different parts of the hole surface are differently inclined with respect to the incident beam. The total profile of the surface of the hole consists of the two main parts [30–33]:

(i) Transient profile where the material is removed to a great extent. The profile of this type corresponds in Fig. 12 to the bottom of the hole and a transition region between the bottom and inclined side walls of the hole.

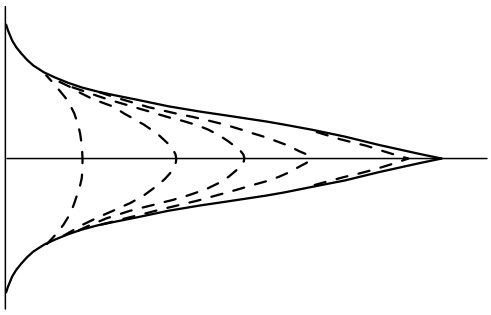

Figure 12. Stationary (solid curves) and transient (dashed curves) parts of the surface profile upon multipulse laser drilling a deep hole.

(ii) Stationary profile where the material is almost not removed and therefore its slope does not change from pulse to pulse. The profile of this type is mainly located on the side walls of the hole in Fig. 12. Its slope is established after irradiation by a certain number of pulses due to self-regulating processes in such a way that the maximum local surface temperature $T_{\mathrm{loc}}(r, z)$ achieved at each point of the profile with coordinates r, z after the action of the laser pulse is constant along this part of the profile:

$$T_{\mathrm{loc}}(r, z) = \mathrm{const} = T_{\mathrm{st}}. \tag{1}$$

This theoretical statement corresponds to the constant depth of the laser-affected region along the side walls of the hole observed in experiments, which was described above (Fig. 11).

The temperature T_{st} in equality (1) corresponds to the achievement of the mobility threshold of the material on side walls in the presence of a strong perturbing ejecting effect of a plasma–vapour plume propagating from the bottom of the hole to its entrance [30, 35], i.e., this is the maximum temperature at which the material is not removed from the side walls. For the laser action in a chemically inert atmosphere considered below, we assume that

$$T_{\mathrm{st}} = T_{\mathrm{m}}, \tag{2}$$

where T_{m} is the melting temperature. This relation means that the melt depth is virtually zero on the side walls [30, 36]. If we assume that higher temperatures $T^* > T_{\mathrm{m}}$ can be achieved in some part of the wall profile, this will provide the appearance of a melt of a certain depth, which can be removed from side walls in the presence of a plasma–vapour flow. One of the possible mechanisms of such a removal can be the 'entrainment' of the melt by a powerful vapour flow along the walls toward the exit from the hole. A part of the melt can be ejected outside under the action of one or several successive pulses.

An additional or alternative mechanism (especially for high-viscosity materials with a low mobility of the melt, to which, unlike metal melts, belong polymer and ceramic melts) can be the formation of only a melt fold on the wall by a powerful vapour flow moving tangentially from the bottom outside. The incidence of laser radiation on such a fold is no longer grazing, as for the rest part of the side wall, which results in a drastic increase in the energy density absorbed in this perturbation of the relief [see below expression (6)] and evaporation and (or) sputtering of the melt in the form of droplets. A part of the droplets, which have not escaped outside at once but precipitated on the side walls, also produce a similar perturbation of the relief (the incidence of a laser beam on these droplets is also not grazing, being closer to the normal incidence), and the evaporation and (or) sputtering processes repeat again upon irradiation by the next laser pulses, each time involving a new portion of the material.

Thus, a part of the profile where the temperature exceeds the melting temperature cannot be stationary because here the material is removed.

Drilling in a chemically active medium can be performed at the temperature T_{st} lower than T_{m} because the mobility of a material and its removal from the walls can be achieved at temperatures lower than the melting point due to chemical transformations of the initial material to some intermediate product with different properties. For example, it is known that upon the laser ablation of diamond films in air or oxygen, their graphitisation can occur, which is followed by the formation of volatile oxides CO and CO_2 at temperatures 900–1200 °C, which are considerably lower than the melting and evaporation temperatures (~ 4500 °C). It is also known that upon laser irradiation of vanadium in air, the oxide is formed with the melting temperature which is much lower than that of pure vanadium. This oxide can flow off from the irradiated vanadium surface.

During the deepening of a hole with increasing the number of laser pulses of the same intensity, the transient part of the walls of the hole decreases (therefore, the amount of the material removed per pulse also decreases), whereas the area of the stationary part increases. Eventually the situation appears when the hole depth does not increase or increases only weakly despite further pulsed irradiation (the total surface of the hole becomes stationary, while the transient part almost disappears), which corresponds to the deepest hole in Fig. 12. Thus, we can assume that the final shape of the side walls of the hole is determined by the stationary profile. This well agrees with the above-described experimental observation of the spontaneous stop of drilling when the hole achieves a certain depth (stage III in Fig. 6).

Therefore, we will consider below only this type of the profile because it determines the final parameters of the hole such as the slope of the side walls, the saturated depth, and the aspect ratio.

Below, we use in simulations the following assumptions:

(i) The side walls are heated only due to absorption of the incident radiation, while the contribution of a plasma plume to the heating of the walls is neglected;

(ii) the attenuation of laser radiation incident on the side walls of a deep hole due to absorption in the plasma ablation plume is neglected.

In the case of drilling deep holes (5–22 mm) considered here, screening can be mainly caused by the part of the plasma plume that was formed in the transient part of the profile where the rate of material removal is maximal and, therefore, the plume density is also maximal, i.e., on the bottom of the hole and probably in the intermediate region between the bottom and the stationary part of the profile on the side walls (Fig. 12). However, this most dense part of the plume remains localised near the bottom within a narrow region of thickness 0.1–0.2 mm corresponding to the characteristic distance $v_p\tau$ over which the plasma plume propagates from the bottom of the hole during the laser pulse of duration $\tau = 20 - 30$ ns for the typical propagation velocity of the plasma $v_p \simeq (1.5 - 5) \times 10^5$ cm s^{-1}. This means that this part of the plume near the bottom almost does not attenuate radiation incident on the main part of the side walls which is located a few millimetres above of the near-bottom region. Generally speaking, another part of the plume can be formed on the side walls. However, when the profile of the side walls irradiated by repeated pulses becomes close to the stationary profile, the evaporation of the wall material is almost absent or is very weak compared to that from the bottom because the energy density absorbed in this part of the profile becomes close to the melting threshold F_{ma} (when $T_{st} = T_m$) or the evaporation threshold F_{va} (when $T_{st} = T_b$, where T_b is the boiling temperature). Thus, in any case the stationary part of the surface of the hole is not evaporated in fact and therefore a laser plume that would cause a considerable screening cannot be formed.

Upon pulsed heating, when $1/\gamma, (\chi\tau)^{1/2} \ll r, h$ (where r is the radius of the hole, h is its depth, and γ and χ are the absorption coefficient (in cm^{-1}) and thermal diffusivity of the target material), the isothermal property (1) of the stationary profile corresponds to its 'isoabsorption' property, i.e., to a constant energy density F_a absorbed along this part of the profile:

$$F_a(r, z) = \text{const} = F_{st}, \tag{3}$$

where F_{st} is the threshold density of absorbed energy corresponding to the surface temperature $T = T_{st}$. For the surface heating ($\gamma^2\chi\tau > 1$) corresponding to the heating of metals drilled by 20–30-ns pulses, we have for $T_{st} = T_m$:

$$F_{st} = \frac{1}{2}(\pi\chi\tau)^{1/2}\rho[C(T_m - T_i) + L_m], \tag{4}$$

where C and ρ are the specific heat (in J g^{-1} K^{-1}) and density (in g cm^{-3}) of the material, respectively; L_m is the latent heat of melting; and T_i is the initial temperature of the environment. At the same time, upon bulk heating ($\gamma^2\chi\tau < 1$), which is more appropriate for drilling polymers by nanosecond pulses, when it makes sense to say about melting, we can assume that $T_{st} = T_m$ and then

$$F_{st} = \frac{C(T_m - T_i) + L_m}{\gamma}. \tag{5}$$

In the model of multipulse drilling considered here, we assume for simplicity that T_i does not change in time, i.e., the material has time to cool almost completely by the arrival of each next pulse. This assumption is valid for a low repetition rate (10–20 Hz) of nanosecond pulses used for drilling.

With the above assumptions neglecting plasma heating, the expression for the radiation energy density absorbed in the side walls can be written in the form

$$F_a(r, z) = A[\varphi(r, z)]F(r, z)\sin\varphi(r, z), \tag{6}$$

where $F(r, z)$ is the incident energy density at the point P of the profile with coordinates r, z (Fig. 2b) and $A[\varphi(r, z)]$ is the absorptivity of the material. The expression for the axially symmetric distribution of the energy density $F(r, z)$ in the beam can be written in the general form

$$F(r, z) = \frac{F(\alpha)}{\cos\alpha}\frac{z_0^2 + r_1^2}{z^2 + r^2}, \tag{7}$$

where α is the slope of the beam OP with respect to the optical axis z and $F(\alpha)$ is the angular axially symmetric distribution of the radiation energy density on the front surface $z = z_0$ of a sample. We assume that $F(\alpha)$ can be inhomogeneous in the general case. Then, $F(\alpha)/\cos\alpha$ is the energy density in the cross section perpendicular to the beam OP at the point (r_1, z_0) at the entrance to the hole. The factor $(z_0^2 + r_1^2)/(z^2 + r^2)$ takes into account a decrease in the energy density with increasing distance $\xi = (z^2 + r^2)^{1/2}$ from the point O as $1/\xi^2$. For a paraxial beam, we have $(\alpha \ll 1)\cos\alpha \simeq 1$. In addition, it follows from obvious geometrical relations (Fig. 2b) that $(z_0^2 + r_1^2) \times (z^2 + r^2)^{-1} = z_0^2/z^2$. Then, the expression for $F(r, z)$ takes the form

$$F(r, z) = \frac{F(\alpha)z_0^2}{z^2}. \tag{8}$$

In expression (6), $\varphi(r, z)$ is the grazing angle of the beam OP with respect to the surface at the point P. As follows from obvious geometrical relations (Fig. 2b),

$$\varphi(r, z) = \alpha(r, z) - \beta(r, z), \tag{9}$$

where $\beta(r, z)$ is the local slope of the side walls of the hole at the point (r, z). In the paraxial optics approximation (α, β, $\varphi \ll 1$), we have

$$\alpha = \arctan\frac{r}{z} \simeq \frac{r}{z}, \qquad \beta = \arctan\frac{dr}{dz} \simeq \frac{dr}{dz}. \tag{10}$$

Because $r = \alpha z$, the latter relation takes the form

$$\beta \simeq \frac{d(\alpha z)}{dz} = \alpha + z\frac{d\alpha}{dz}. \tag{11}$$

By substituting (11) into (9), we find $\sin\varphi$ as a function of z and α:

$$\sin\varphi(r,z) \simeq \varphi(r,z) = -z\frac{\mathrm{d}\alpha}{\mathrm{d}z}. \tag{12}$$

The absorptivity $A[\varphi(r,z)]$ in (6) depends on a particular mechanism of propagation and absorption of laser radiation inside the hole. This mechanism depends in turn on the state of the side-wall surface. We will estimate $A[\varphi(r,z)]$ for two limiting cases.

(i) The specular reflection model. In this case, the side walls are assumed smooth enough so that the rays coming from a point source O are reflected from them in a specular way. Further multiple reflections inside the hole are neglected. For grazing angles $\varphi \sim 1/200 - 1/600$ rad (corresponding to the aspect ratios of the holes considered here equal to 100–300), the absorptivity $A(\varphi)$ calculated by Fresnel formulas is $2n\varphi$ (n is the real part of the complex refractive index) and proves to be very small for the angles φ considered here: $A = 0.005 - 0.05$. As a result, the calculation of the hole depth as a function of the laser energy density in the specular reflection model gives values that are 10–30 times lower than experimental values, whereas the calculations in the multiple scattering model (see below), in which $A = 1$, well agree with the experiment. Therefore, we will not consider the specular reflection model below.

(ii) The multiple scattering model (Fig. 13). This model assumes that the side walls strongly scatter the rays coming from a point source O due to their roughness caused by the precipitation of vapour and droplets escaped from the bottom and side walls and (or) by perturbations and channeling of a melted layer on the side walls due to its interaction with a strong vapour–plasma flow propagating from the bottom of the hole toward its entrance, and (or) the contraction of the hole profile upon cooling after each laser pulse. In this case, $A[\varphi(r,z)]$ is the local effective absorptivity for a superhigh-aspect-ratio hole taking into account multiple reflections and absorptions of the beam OP incident on the surface at the grazing angle φ. After the first contact with the side walls, the beam OP (Fig. 13) is scattered into many secondary rays propagating in different directions. The main part of these rays is incident on the opposite wall already not at grazing angles but at the angles close to the normal incidence, for which the absorptivity $A = 1 - R$ (where R is the reflection coefficient) of polymers is very high (about 95 %). This means that only one or two successive reflections and scatterings of these rays from side walls are sufficient to provide virtually complete absorption of the initial beam OP in a short region near the point P. One can see from Fig. 13 that the length L of this region of diffuse absorption along the hole axis (which can be also called the length of the 'waveguide' radiation energy transfer along the hole) does not exceed several diameters d of the hole near the point P: $L = (2-4)d$. However, the total depth h of high- and superhigh-aspect-ratio holes considered here is much greater: $h = (200 - 600)d$, i.e., $L \ll h$, which is also valid for any other neighbouring initial rays coming from a point source. Therefore, we can assume that the total effective absorptivity at each point of the profile along the length of the hole is

$$A(\varphi(r,z)) = A_{\mathrm{eff}}(\varphi(r,z)) \simeq 1. \tag{13}$$

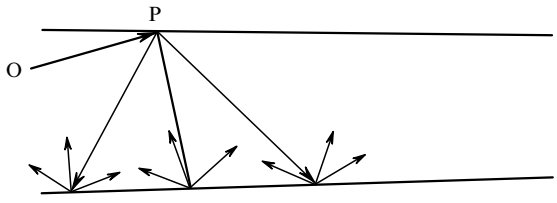

Figure 13. Scheme illustrating the multiple scattering model. The initial ray OP (one of the many rays of the laser beam) incident on the laser hole surface at the glancing angle is diffusively reflected several times from the wall and is absorbed

Thus, in this model the hole is filled with scattered diffused radiation, and scattered rays are incident from the left and right at different angles on each point of the stationary profile, thereby providing local absorption and heating. The only exception is small regions of length approximately L directly adjacent to the entrance and bottom (end) of the hole where scattered beams can come only from one side. Therefore, it is expected that local absorptivity in these regions is less approximately by half than absorptivity (13).

By substituting (8), (12), and (13) into (6), we can rewrite the 'isoabsorption' condition (3) in the form of an ordinary differential equation for the stationary profile of the hole:

$$z\frac{\mathrm{d}z}{\mathrm{d}\alpha} = -\frac{z_0^2}{F_{\mathrm{st}}}F(\alpha) \tag{14}$$

with the boundary condition $z(\alpha = \alpha_\infty) = z_0$. Here, α_∞ is a certain limiting angle in the angular distribution of the incident laser beam above which the beam intensity on the front plane of a sample becomes so small that its contribution to the removal of the material from the surface can be neglected. The solution $z(\alpha)$ of Eqn (14) gives the parametric dependences (where the parameter is α) of the profile $r(z)$ and depth h of a final hole on the laser energy density:

$$z(\alpha) = z_0\left[1 + \frac{2}{F_{\mathrm{st}}}\int_\alpha^{\alpha_\infty} F(\alpha')\mathrm{d}\alpha'\right]^{1/2},\ r(\alpha) = \alpha z(\alpha) \tag{15}$$

$$(0 \leqslant \alpha \leqslant \alpha_\infty,\ z_0 \leqslant z \leqslant h),$$

$$h(F) = z(\alpha = 0) - z_0$$

$$= z_0\left\{\left[1 + \frac{2}{F_{\mathrm{st}}}\int_\alpha^{\alpha_\infty} F(\alpha')\mathrm{d}\alpha'\right]^{1/2} - 1\right\}. \tag{16}$$

Consider some corollaries of this model.

3.1 Threshold beam energy density required for obtaining parallel side walls at the entrance to a hole

The parallelism of side walls, at least at the entrance $z = z_0$ to a laser hole, i.e., $\beta = \mathrm{d}r/\mathrm{d}z = 0$ for $z = z_0$ is provided when the energy density $F(\alpha_0)$ at the spot boundary ($\alpha = \alpha_0$) in the input plane of a sample achieves the threshold F_{par}.

By using (9), we obtain from the condition $\beta(z = z_0) = 0$ that $\varphi(z = z_0) = \alpha_0$, which after substitution into (6), taking (3) into account, gives

$$F_{\text{par}} = \frac{F_{\text{st}}}{\alpha_0}. \tag{17}$$

For $F(\alpha_0) < F_{\text{par}}$, the walls of the hole at the entrance converge into depth, whereas for $F(\alpha_0) > F_{\text{par}}$, they diverge into depth at the entrance, although converge in a deeper part of the hole.

3.2 Distribution of the beam energy density providing strictly cylindrical side walls

The energy density profile $F_{\parallel}(\alpha)$ on the input surface of a sample providing strictly cylindrical side walls over the entire depth during drilling through holes in a plate of thickness h_s can be obtained from Eqn (14) after the substitution of $r(z) = \text{const} = r_0$, $z = r_0/\alpha$, and $r_0/z_0 = \alpha_0$ into it (Fig. 14a) taking (17) into account:

$$F_{\parallel}(\alpha) = \frac{F_{\text{par}}\alpha_0^3}{\alpha^3} \text{ for } \alpha_1 \leqslant \alpha \leqslant \alpha_0,$$
$$F_{\parallel}(\alpha) = 0 \text{ for } \alpha \geqslant \alpha_0. \tag{18}$$

Here, $\alpha_1 = r_0/(z_0 + h_s)$ is the angle at which the output aperture of the hole (for $z_1 = z_0 + h_s$) is seen from the point source O. It follows from Fig. 14b that the obtained energy density distribution $F_{\parallel}(\alpha)$ drastically increases with decreasing α (as $1/\alpha^3$), i.e., it should be strongly concentrated near the optical axis, at least in the angular range $\alpha_0 \geqslant \alpha \geqslant \alpha_1$. The details of the behaviour of the distribution $F_{\parallel}(\alpha)$ for $\alpha < \alpha_1$ are, strictly speaking, not important because beams with $\alpha < \alpha_1$ propagate in a through hole in its final stationary state without contact with its side walls.

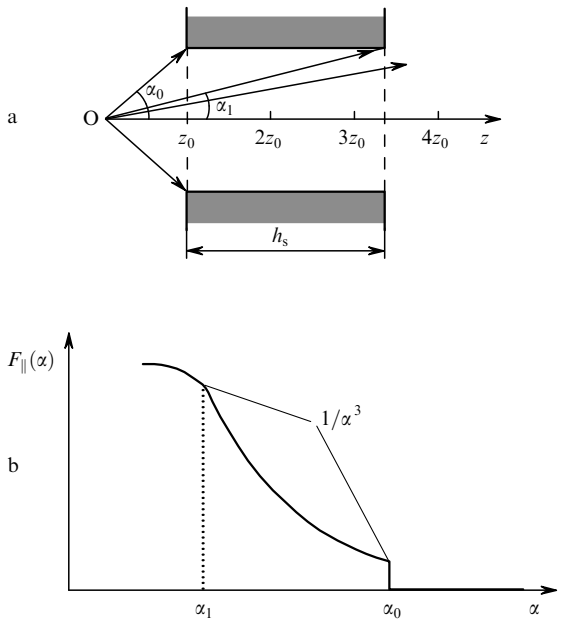

Figure 14. Strictly cylindrical hole profile [$r(z) = \text{const} = r_0$] in a sample of thickness h_s (a) provided by the optimised energy density distribution: $F_{\parallel}(\alpha) = F_{\text{par}}(\alpha_0/\alpha)^3$ for $\alpha_1 \leqslant \alpha \leqslant \alpha_0$ and $F_{\parallel}(\alpha) = 0$ for $\alpha > \alpha_0$ (b). All the angles in Fig. 14a are strongly enlarged for clearness.

3.3 Shape of a hole for the rectangular energy density distribution

For the rectangular energy density distribution at the input plane of a sample

$$F(\alpha) = \begin{cases} \text{const} = F & \text{for } \alpha \leqslant \alpha_0, \\ 0 & \text{for } \alpha > \alpha_0, \end{cases}$$

which is typical for irradiation by an excimer laser by using a projection scheme, relations (15) for $r(\alpha)$ and $z(\alpha)$ upon the substitution $\alpha_\infty = \alpha_0$ give the explicit dependence $r(z)$:

$$r(z) = c_1 z - c_3 z^3, \tag{19}$$

where

$$c_1 = \frac{\alpha_0(1 + 2\psi)}{2\psi};\ c_3 = \frac{\alpha_0}{2z_0^2\psi};\ \psi(F) = \frac{F}{F_{\text{par}}}.$$

The particular shape of a drilled hole is determined by the laser energy density because coefficients c_1 and c_3 depend on F. Profiles of the holes calculated for different F presented in Fig. 15 show that the holes can not only converge into depth but also diverge (at least, near the entrance).

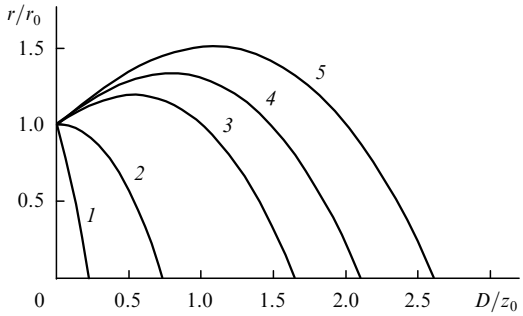

Figure 15. Calculated stationary profiles of holes for a beam with the rectangular intensity distribution for $F/F_{\text{par}} = 0.25$ (*1*), 1 (*2*), 3 (*3*), 4.3 (*4*), and 6 (*5*) (where $F_{\text{par}} = F_{\text{st}}z_0/r_0$ is the threshold energy density at the spot boundary $r = r_0$ providing the parallelism of side walls at the hole entrance, r_0 is the beam radius on the input plane of a sample). A point source irradiating the surface is located at the point $z = 0$; the sample is located in the region $z \geqslant z_0$ (i.e., $D/z_0 \geqslant 0$, where $D = z - z_0$).

A simple mathematical dependence $r(z)$ allows us to find all the characteristic points and parameters of the profile:

$$z_1 = z_0(1 + 2\psi)^{1/2},\ z_{\max} = \frac{z_1}{\sqrt{3}},\ r_{\max} = \frac{r_0(1 + 2\psi)^{3/2}}{3\sqrt{3}\psi}, \tag{20}$$

$$h(F) = z_0\left[(1 + 2\psi)^{1/2} - 1\right] = z_0\left[\left(1 + \frac{2Fr_0}{F_{\text{st}}z_0}\right)^{1/2} - 1\right], \tag{21a}$$

or

$$h(F) = z_0\left[\left(1 + \frac{2F\gamma r_0}{C\rho(T_{\text{m}} - T_{\text{i}})z_0}\right)^{1/2} - 1\right], \tag{21b}$$

$$\beta(z = z_0) = \frac{\alpha_0(\psi - 1)}{\psi}. \tag{22}$$

Here, z_1 is the position of the end of a 'blind' (non-through) hole obtained from the condition $r(z_1) = 0$; r_{max} is the maximum (depending on z) radius of the profile for $\psi \geqslant 1$; z_{max} is the position of the maximum radius $r = r_{max}$ of the profile obtained from the condition $dr/dz = 0$ for $z = z_{max}$; h is the depth of the hole drilled; and $\beta(z = z_0)$ is the local slope of side walls at the entrance.

These expressions [in particular, (21b)] demonstrate explicitly the controlling factors of drilling: material parameters (C, r, T_m, T_i, γ), geometrical focusing parameters z_0 and r_0, and laser parameters (F). The analyticalal dependence (21a) of the hole depth on the laser energy density well agrees with the experimental data (Fig. 9) obtained for all polymers studied. The best fit was achieved for $F_{st} = 1$, 2.2, 3, 5, 6.6, and 8.5 mJ cm^{-2} for PET, PC, PI, PS, PMMA, and PEEK, respectively. Note that the two other parameters z_0 and r_0 in (21a) were taken identical ($z_0 = 1.8$ mm and $r_0 = 30$ μm) to obtain the best fit for all the polymers.

One can see from (22) that side walls at the entrance are parallel [$\beta(z = z_0) = 0$] for $\psi = 1$, i.e., $F = F_{par}$ [curve (*2*) in Fig. 15]. For the energy density lower than the threshold ($F < F_{par}$), the hole converges into depth over its entire length: $\beta(z \geqslant z_0) < 0$ [curve (*1*) in Fig. 15], whereas for the energy density above the threshold ($F > F_{par}$), the side walls at the entrance diverge [$\beta(z = z_0) > 0$], although later their slope decreases and becomes negative, i.e., the profile converges at depths $z > z_{max}$ [curves (*3–5*) in Fig. 15].

3.4 Drilling deep through holes with a diameter weakly varying along the hole length by laser beams with the rectangular energy density distribution

One can see from Fig. 15 that the obtained profiles have no strictly parallel walls as in the case of the optimised energy density distribution (18). As the energy density is increased, the coordinate $z = z_{max}$ of the maximum radius r_{max} of the profile shifts to larger values of z and for $F \geqslant F_{par}$ it is located inside the material [curves (*3–5*) in Fig. 15]. Near $z = z_{max}$, the hole diameter changes with z to the least degree. For each energy density, a region of depths inside the profile can be found where the change in the hole radius $r(z)$ from its maximum value r_{max} to the minimum value r_{min} does not exceed, for example, 33.3 %, i.e., $r_{max}/r_{min} \leqslant 1.33$. The length H of this region depends on the energy density F, and the maximum value of $H(F)$ denoted by H_{opt} is achieved, as follows from calculations, for

$$F = F_{opt} = 8.6 a_0 F_{st} \tag{23}$$

and is

$$H_{opt} = 1.48 z_0. \tag{24}$$

Here, $a_0 = z_0/(2r_0) = 1/(2\alpha_0)$ is the geometrical parameter determined by the beam focusing on the surface. This parameter has the physical meaning of the inverse angular divergence of the beam behind the waist. Therefore, when the sample thickness h_s is chosen so that

$$h_s = H_{opt}, \tag{25}$$

we can obtain through holes close to cylindrical ones with the aspect ratio

$$a_{opt} = 1.48 a_0. \tag{26}$$

The substitution of the experimental values $a_0 = 60$ and $F_{st} \simeq 1$ mJ cm^{-2} for PET (Fig. 9) gives the estimate $a_{opt} = 89$ for $F = F_{opt} = 0.52$ J cm^{-2}.

One can see that the aspect ratio a_{opt} is proportional to the inverse angular divergence a_0. It is known from optics that $2\alpha_0$ can be simply estimated as $2\alpha_0 = \lambda/d_f$, where d_f is the beam waist diameter, therefore, $a_0 = d_f/\lambda$. When the input plane is located outside the waist, so that, for example, $d = 2d_f$, we have

$$a_0 = \frac{d}{2\lambda}.$$

Thus, a_0 increases with increasing d and decreasing λ. In the experiments described above, $d = 30$ μm and $\lambda = 248$ nm, which gives $a_0 = 60$. However, by using, for example, $d = 150$ μm and $\lambda = 193$ nm, we obtain much higher value $a_0 = 390$, and according to (26), the aspect ratio of the hole with virtually parallel walls is $a_{opt} = 580$.

3.5 Profile of a hole for a Gaussian beam

An important practical case is drilling by a Gaussian beam (Fig. 16). The angular distribution of the beam energy density on the input plane of a sample in the model considered below is described by the expression

$$F(\alpha) = F \exp\left(-\frac{2\alpha^2}{w_\alpha^2}\right), \tag{27}$$

where w_α is the angular divergence of a Gaussian beam. In Fig. 16, $z = 0$ is the coordinate of the beam waist, w_0 is the waist radius, $z = z_0$ is the position of the front plane of the sample, the material is located in the region $z \geqslant z_0$, and $z_R = \pi w_0^2 \lambda^{-1}$ is the so-called Rayleigh length.

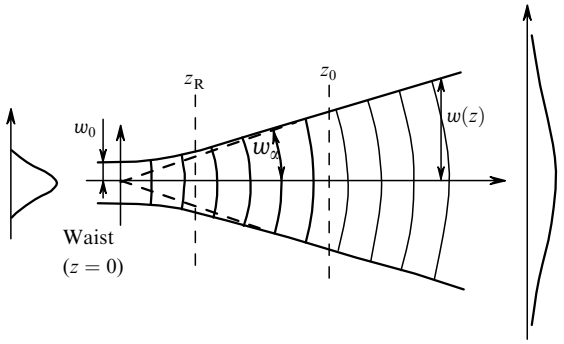

Figure 16. Schematic view of a Gaussian beam used in the drilling model.

We assume for convenience that $z_0 > z_R$. This means that the position of the input plane of the sample is chosen behind the waist in the region where a Gaussian beam can be treated as a spherical wave from a point source located at the point $z = 0$. Under such conditions, the spatial distribution of the energy density $F(r, z)$, taking into account the angular divergence, is described by expression (8) in which $F(\alpha)$ is described by (27).

By substituting (27) into (14) and (15), we can find the profile $r(z)$ of the hole in the parametric form, as well as the final stationary depth of the hole as functions of the energy density of the Gaussian beam:

$$r(\alpha) = \alpha z(\alpha),\ z(\alpha) = z_0\left[1 + \frac{\sqrt{\pi} w_\alpha F}{\sqrt{2} F_{st}} \operatorname{erfc}\left(\frac{\sqrt{2}\alpha}{w_\alpha}\right)\right]^{1/2} \quad (28)$$

$$(0 \leqslant \alpha \leqslant 3w_\alpha),$$

$$h(F) = z_0\left[\left(1 + \frac{\sqrt{\pi} w_\alpha F}{\sqrt{2} F_{st}}\right)^{1/2} - 1\right]. \quad (29)$$

It is interesting to note that the latter expression for $h(F)$ coincides with an accuracy to coefficients with expression (21a) obtained above for a beam with the rectangular distribution of the energy density.

The dimensionless stationary profiles calculated from (28) are shown in Fig. 17 for a number of energy densities. Here, $r_0 = \sqrt{2} w_\alpha z_0$ is the characteristic measurement unit of the radius. One can see that variations in the input energy density F from $0.25F_{opt}$ to $4.5F_{opt}$ (i.e., by 18 times) does not change strongly the hole radius on the input surface $z = z_0$, which is approximately r_0. By dividing expression (29) for the hole depth $h(F)$ on the approximately constant input diameter $2r_0$, we obtain the approximate estimate of the aspect ration $a(F)$ of the hole:

$$a(F) \simeq \frac{h(F)}{2r_0} = a_0\left[\left(1 + \frac{\sqrt{\pi}_\alpha F}{\sqrt{2} F_{st}}\right)^{1/2} - 1\right], \quad (30)$$

where

$$a_0 = \frac{z_0}{2r_0} = \frac{1}{2\sqrt{2} w_\alpha} \quad (31)$$

can be called the aspect ratio of the laser Gaussian beam itself.

For superhigh aspect ratios, we have $\sqrt{\pi} w_\alpha F \times (\sqrt{2} F_{st})^{-1} \gg 1$. Then, expression (30) takes the form

$$a(F) \simeq \frac{\pi^{1/4}}{2 \times 2^{3/4}} \left(\frac{1}{w_\alpha} \frac{F}{F_{st}}\right)^{1/2}. \quad (32)$$

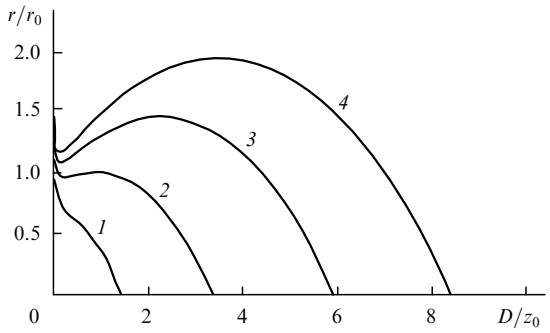

Figure 17. Calculated dimensionless stationary hole profiles for a Gaussian beam with the energy density distribution $F(\alpha) = F \times \exp(-2\alpha^2/w_\alpha^2)$ for $F/F_{opt} = 0.25$ (*1*), 1 (*2*), 2.43 (*3*), and 4.5 (*4*); $F_{opt} = 15.4F_{st}/w_\alpha$, $r_0 = \sqrt{2} w_\alpha z_0$.

One can see from (32) that to drill superhigh-aspect-ratio holes (several hundreds), the relation

$$\frac{1}{w_\alpha} \frac{F}{F_{st}} = 10^5 - 10^6 \quad (33)$$

should be fulfilled, which can be obtained when the laser energy density greatly exceeds the threshold of material removal in the absence of heating walls by the plasma ($F/F_{st} = 10^3 - 10^4$, which is fulfilled for polymers) and the divergence of the laser beam is low ($w_\alpha = 10^{-2} - 10^{-3}$).

Let H be the length of the hole region where the change in the radius from its maximum value r_{max} in this region to its minimum value r_{min} does not exceed 5 % (i.e., $r_{max}/r_{min} \leqslant 1.05$). The length H is small for small F, when the hole rapidly converges into depth [as, for example, for curve (*1*) in Fig. 17] and for large F, when the hole rapidly diverges into depth, at least, near the input [as, for example, for curves (*3*) and (*4*)]. Therefore, the maximum value $H_{opt} = 1.66z_0$ is achieved for some optimal energy density $F_{opt} = 15.4F_{st}/w_\alpha$ corresponding to profile (*2*) in Fig. 17. Similarly to the above-considered case of the beam with the rectangular distribution of the energy density, by selecting the sample thickness $h_s = H_{opt}$, we obtain a through hole close to a cylindrical hole with the aspect ratio

$$a_{opt} = 1.66a_0. \quad (34)$$

For example, by substituting the experimental value $a_0 = 60$, we obtain $a_{opt} = 100$.

3.6 Calculation of the transmission of laser beam in through holes depending on their depth. Comparison with experiments

In our polymer drilling model, all the rays propagating from a point source to side walls are completely absorbed due to multiple scatterings upon reflections from the walls. In the case of superhigh-aspect-ratio holes, waveguide effects prove to be insignificant in the radiation energy transfer along the hole axis because, as shown above, the characteristic length L of the 'waveguide' energy transfer along the hole is much smaller than a final depth h of the hole. Therefore, we can assume that the transmission of a through hole is determined only by the energy of rays from a point source O directly propagated to the output cross section of the through hole.

Let us verify the validity of this statement by considering the experimental measurements of the transmission of a laser beam by through holes of different lengths described in section 2 and presented in Fig. 10. The energy of a beam with the rectangular energy distribution $E(z)$ transmitted through a hole is directly proportional to the solid angle Ω at which the output aperture is seen from a point source:

$$E(z) \propto \Omega(z) = \frac{\pi r^2(z)}{z^2}.$$

The energy E_0 of the incident laser beam can be written in the form

$$E_0 \propto \Omega_0 = \frac{\pi r_0^2}{z_0^2}.$$

Therefore, the transmission $T(z) = E(z)/E_0$ is

$$T(z) = \frac{r^2(z)}{z^2}\frac{z_0^2}{r_0^2}, \tag{35}$$

where the hole profile $r(z)$ is described by expression (19).

The calculation for a Gaussian beam is somewhat more complicated because the dependence $T(z)$ is described in the parametric form, where the parameter is the angle α:

$$T(\alpha) = 1 - \exp\left(-\frac{2\alpha^2}{w_\alpha^2}\right),$$
$$z(\alpha) = z_0\left[1 + \frac{\sqrt{\pi}w_\alpha F}{\sqrt{2}F_{st}}\operatorname{erfc}\left(\frac{\sqrt{2}\alpha}{w_\alpha}\right)\right]^{1/2} \quad (0 \leqslant \alpha \leqslant 3w_\alpha). \tag{36}$$

Figures 18 and 19 show the transmission of a through hole calculated from (35) and (36) as a function of the dimensionless hole depth for the rectangular and Gaussian beams for low and high laser energy densities. The hole profiles are also presented in the figures. One can see that in the main part of the hole, except a relatively small part of its length directly adjacent to the bottom, the dependence $T(z)$ is close to linear both for the rectangular and Gaussian beams, irrespective of the particular hole profile and energy density. This well agrees with the experimental transmission discussed above (Fig. 10), which also linearly decreases with increasing the depth of the hole. This agreement between the model and experiment indirectly confirms our assumption that the contribution of waveguide effects to energy transfer along the hole axis upon drilling superhigh-aspect-ratio holes in polymers by UV laser pulses is insignificant.

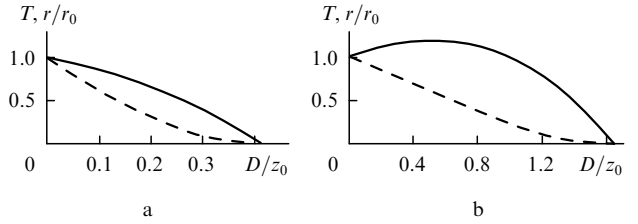

Figure 18. Transmission of the laser energy by a through hole (dashed curves) as function of the dimensionless depth of the hole for a beam with the rectangular profile for $F/F_{par} = 0.5$ (a) and 3 (b). The corresponding hole profiles are shown by the solid curves.

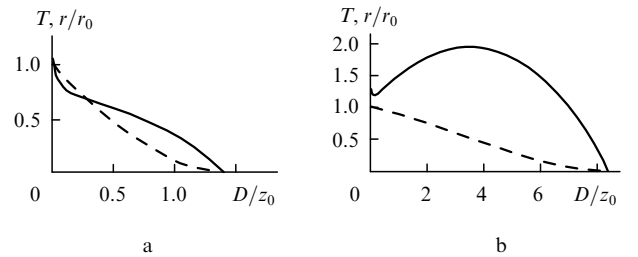

Figure 19. Transmission of the laser energy by a through hole (dashed curves) as a function of the dimensionless depth of the hole for a Gaussian laser beam with the energy density distribution $F(\alpha) = F\exp(-2\alpha^2/w_\alpha^2)$ for $F/F_{opt} = 0.25$ (a) and 4.5 (b); $F_{opt} = 15.4F_{st}w_\alpha^{-1}$. The corresponding hole profiles are shown by the solid curves.

4. Discussion of results

The energy density of the incident laser beam on the front surface of a sample upon drilling is 7–10 J cm^{-2}, which exceeds by many times the ablation threshold of the sample material. During the movement of the ablation front deep in the material, the radiation energy density achieving the hole bottom decreases especially for deep holes with a very high aspect ratio. Our model takes into account the angular divergence of radiation and its attenuation with distance – the important factors controlling the final stationary profile of the deep hole.

Ablation and drilling stop spontaneously because the laser energy absorbed in walls becomes equal to (or lower than) a threshold F_{st}, which we call the threshold of material removing from side walls to avoid confusion with the classical ablation threshold F_{th} in shallow spots. These thresholds are presented in Table 1. It is interesting that F_{st} for polymers under study is systematically much lower than F_{th}. The reason is the different mechanism of material removal from side wall upon drilling than upon ablation from a shallow spot. In particular, the ejection of a melt makes an important contribution. One can see from Fig. 5b that the entrance to the hole in PMMA is covered by numerous deposited droplets. The removal of the material from a shallow spot upon usual ablation is caused only the expansion of the volume excited by a laser. Upon ablation from a deep hole, the flow of the material in the form of a gas and liquid and solid particles propagates from the bottom to the entrance. As a result, any elementary surface on the side walls of the hole experiences a strong 'entraining' influence of the gas flow toward the entrance. This makes the material removal more efficient upon drilling holes than upon usual surface ablation from a shallow spot. In other words, the material removal is favoured by additional factors such as a plasma flow and a shock wave propagating from the bottom of the hole to its entrance. To understand in detail processes occurring in the hole during pulsed ablation, further investigations are required. In addition, polymers differ from metals by a higher viscosity in melts and are generally less sensitive to the melt movement along the surface. PMMA represents the limiting case: the melt of this polymer produced by irradiation at 248 nm is very abundant. Another limiting case is PC which produces manly gas upon ablation. The intermediate situation is observed for PET for which we measured recently [37, 38] the melt flow upon ablation by microbeams.

The use of a large focal distance f results in an increase in the aspect ratio of a beam according to a simple relation $a_0 \propto f/D_0$, where D_0 is the beam diameter on a projecting lens (see Fig. 2a). As follows from (26) and (30), the aspect ratio of a part of the hole with a constant diameter increases with a_0. However, the optimal energy density F_{opt} required for obtaining such holes, which also increases with increasing a_0, can exceed the characteristic threshold F_{pl} above which the influence of the plasma on the broadening of the hole profile becomes significant. To avoid this, it is reasonable to limit a_0 so $(a_0 \leqslant a_0^{max})$ as to obtain $F_{opt}(a_0^{max}) \approx F_{pl}$. By using (23), we obtain from the latter relation that $a_0^{max} = F_{pl}/(8.6F_{st})$, which, according to (26), set the limit $a_{opt}^{max} = F_{pl}/(5.8F_{st})$ for the maximum aspect ratio for the part of the hole with a constant diameter. This simple relation shows that the value of a_{opt}^{max} can be increased either by

(i) increasing F_{pl}, for example, by using shorter-wavelength radiation or performing irradiation in vacuum or

(ii) decreasing F_{st}, for example, as follows from (5), by increasing the absorption coefficient γ of the polymer using the proper laser wavelength and (or) doping the polymer with strongly absorbing impurities. In addition, irradiation can be performed in a chemically active medium and the initial temperature T_i of the sample can be increased, which could be especially efficient upon drilling metals and ceramics.

These optimised aspect ratios were obtained here in the case of the immobile beam waist with respect to the material. Aspect ratios can be considerably (by several times) increased by using a more complicated drilling 'strategy', for example, by gradually moving the beam waist along the hole axis deep in the material. This allows one to increase the length of the part of the hole with a constant diameter.

Finally, the authors of paper [29] have assumed earlier that a high aspect ratio of the hole drilled by a laser in their experiments can be explained by the efficient radiation channeling in the hole. It is interesting that the model of multiple scattering and absorption of radiation proposed in our paper quantitatively explains drilling high-aspect-ratio holes in polymers but does not confirm the possibility of radiation channeling (Fig. 9). Therefore, we believe that the waveguide effect is insignificant for energy transfer along the hole during drilling high-aspect-ratio holes, at least in our particular case of UV LD of polymers.

5. Conclusions

Based on systematic experimental studies, the analyticalal model of drilling superhigh-aspect-ratio (several hundreds) holes in polymers irradiated by a repetitively pulsed excimer KrF laser has been constructed. The model uses the concept of surface self-organisation: the surface relief irradiated by repeated intense laser pulses undergoes the transition to a new, more stable state, which corresponds to the final stationary profile of a deep laser hole.

The following results have been obtained:

(i) A particular mechanism of propagation and absorption of energy in deep holes has been proposed. This mechanism, taking into account the angular divergence of a focused laser beam, forms the basis of the theoretical description of laser drilling deep holes.

(ii) It has been shown that the calculated dependence of the hole depth on the incident radiation energy density well agrees with the experimental dependence for a laser beam with the rectangular intensity distribution. The final profile of the hole as a function of the incident energy density has been also calculated for a Gaussian laser beam.

(iii) The model shows that, to obtain holes with the aspect ratio of several hundreds, it is necessary to provide the value of $F/(w_\alpha F_{st})$ of the order of $10^5 - 10^6$, which is realised, for example, for polymers for $F/F_{st} = 10^3 - 10^4$ and $w_\alpha = 10^{-2} - 10^{-3}$.

(iv) The expression has been obtained for the optimal laser pulse energy density at which the length of a part of the hole where the hole diameter changes relatively weakly (for example, deviates no more than by $\pm 5\,\%$ from its average value over this length) achieves its maximum. This optimal energy density is directly proportional to the threshold of material removal from the side walls of the hole and is inversely proportional to the angular divergence of the laser beam.

Note also that the optimised aspect ratios obtained here for a simple situation of an immobile beam waist with respect to the irradiated material can be further increased by several times by using a more complicated drilling 'strategy' involving a gradual movement of the beam waist along the hole axis deep in the material.

References

1. Braren B., Srinivasan R. *J. Vac. Sci. Technol. B*, **3**, 913 (1985).
2. *Lambda Highlights*, **7**, 4 (1987).
3. Liedl G., Schröder K., Kaplan A.F.H. *Appl. Surf. Sci.*, **106**, 374 (1996).
4. *Lambda Highlights*, **18**, 2 (1989).
5. Miyamoto I., Maruo H. *Proc. SPIE Int. Soc. Opt. Eng.*, **1279**, 66 (1990).
6. *Lambda Highlights*, **34**, 2 (1992).
7. Tönshoff H.K., Hesse D., Gedrat O. *Proc. SPIE Int. Soc. Opt. Eng.*, **1810**, 572 (1993).
8. Tsetseku A., Zambetakis Th., Stournaras C.J. *Proc. SPIE Int. Soc. Opt. Eng.*, **1810**, 615 (1993).
9. Kononenko T.V., Garnov S.V., Pimenov S.M., Konov V.I., Dausinger F. *Proc. SPIE Int. Soc. Opt. Eng.*, **3343**, 458 (1998).
10. Wehner M. In: *Werkstoffbearbeitung mit Laserstrahlung*. Ed. by G.Herziger, P.Loosen (München: Carl Hanser Verlag, 1993) p. 180.
11. Sowada U., Lokai P., Kahlert H.J., Basting D. *Laser und Optoelektronik*, **21**, 107 (1989).
12. Poprawe R., Schulze W., Wehner M. *Opto Elektronik Magazin*, **6**, 70 (1990).
13. Lazare S., Drilhole D., Lopez J., Weisbuch F. *Revue de la Société Francaise du Vide*, **54** (287), 265 (1998).
14. Lazare S., Lopez J., Weisbuch F. *Appl. Phys. A*, **69**, 1 (1999).
15. Lopez J., Lazare S., Champeaux C., Catherinot A. *J. Phys. IV*, **9** (5) 153 (1999).
16. Basiev T.T., Fedin A.V., Gavrilov A.V., et al. *Proc. Int. Conf. on Lasers'98* (Virginia: STS Press, 1998).
17. Basiev T.T., Fedin A.V., Gavrilov A.V., et al. *Proc. SPIE Int. Soc. Opt. Eng.*, **3888**, 685 (2000).
18. Callies G., Schittenhelm H., Berger P., Hügel H. *Proc. VI European Conf. on Laser Treatment of Materials (ECLAT'96)* (Stüttgart, Germany, 1996) Vol. 2, p. 613.
19. Hodapp T.W., Fleming P.R. *J. Appl. Phys.*, **84**, 577 (1998).
20. Wu F., Pilkington R.D. *Proc. SPIE Int. Soc. Opt. Eng.*, **3274**, 306 (1998).
21. Paterson C., Holmes A.S., Smith R.W. *J. Appl. Phys.*, **86**, 6538 (1999).
22. Golubev V.S. *Proc. SPIE Int. Soc. Opt. Eng.*, **3888**, 244 (1999).
23. Golubev V.S., Mirzoev F.Kh. *Pis'ma Zh. Tekh. Fiz.*, **29**, 30 (2003).
24. Anisimov S.I., Imas Ya.A., Romanov G.S., Khodyko Yu.V. *Deistvie lazernogo izlucheniya bol'shoi moshchnosti na metally* (Interaction of High-Power Laser Radiation with Metals) (Moscow: Nauka, 1970).
25. Armon E., Hill M., Spalding I.J., Zvirin Y. *J. Appl. Phys.*, **65**, 5003 (1989).
26. Kar A., Mazumder J. *J. Appl. Phys.*, **68**, 3884 (1990).
27. Olson R.W., Swope W.C. *J. Appl. Phys.*, **72**, 3686 (1992).
28. Solana P., Kapadia P., Dowden J.M., Marsden P.J. *J. Phys. D: Appl. Phys.*, **32**, 942 (1999).
29. Podlesnik D.V., Gilgen H.H., Osgood R.M. *Appl. Phys. Lett.*, **48**, 496 (1986).

30. Tokarev V.N., Kaplan A.F.H. *Lasers in Engineering*, **7**, 295 (1998).
31. Tokarev V.N., Lopez J., Lazare S. *Appl. Surf. Sci.*, **168**, 76 (2000).
32. Tokarev V.N., Lopez J., Lazare S., Weisbuch F. *Appl. Phys. A*, **76**, 385 (2002).
33. Lazare S., Tokarev V.N. *Proc. SPIE Int. Soc. Opt. Eng.*, **5662**, 221 (2004).
34. Lazare S., Lopez J., Turlet J.M., Kufner M., Kufner S., Chavel P. *Appl. Opt.*, **35**, 4471 (1996).
35. Tokarev V.N., Wilson J.I.B., Jubber M.G., John P., Milne D.K. *Diamond and Related Materials*, **4**, 169 (1995).
36. Tokarev V.N., Kaplan A.F.H. *J. Appl. Phys.*, **86**, 2836 (1999).
37. Weisbuch F., Tokarev V.N., Lazare S., Débarre D. *Appl. Surf. Sci.*, **186**, 95 (2002).
38. Weisbuch F., Tokarev V.N., Lazare S., Débarre D. *Appl. Phys. A*, **76**, 613 (2003).